A Near-Infrared Stellar Census of the Blue Compact Dwarf Galaxy VII Zw 403^{-1}

Regina E. Schulte-Ladbeck University of Pittsburgh, Pittsburgh, PA 15260

Ulrich Hopp

Universitätssternwarte München, München, FRG

Laura Greggio

Osservatorio Astronomico di Bologna, Bologna, Italy, and Universitätssternwarte München, München, FRG

Mary M. Crone

Skidmore College, Saratoga Springs, NY 12866

| Received : accepted | | | | |
|---------------------|----------|---|----------|--|
| | Received | • | accepted | |

¹Based on observations made with the NASA/ESA Hubble Space Telescope, obtained at the Space Telescope Science Institute, which is operated by the Association of Universities for Research in Astronomy, Inc., under NASA contract NAS 5-26555.

ABSTRACT

We present near-infrared single-star photometry for the low-metallicity Blue Compact Dwarf galaxy VII Zw 403. We achieve limiting magnitudes of F110W ≈ 25.5 and F160W ≈ 24.5 using one of the NICMOS cameras with the HST equivalents of the ground-based J and H filters. The data have a high photometric precision (0.1 mag) and are > 95% complete down to magnitudes of about 23, far deeper than previous ground-based studies in the near-IR. The color-magnitude diagram contains about 1000 point sources. We provide a preliminary transformation of the near-IR photometry into the ground system.

We investigate the tip-of-the-red-giant-branch method in the J and H bands to provide an empirical distance calibration. Combining our result with globular cluster data as well as stellar-evolution models, we recommend $M_{H,TRGB} = -5.5(\pm 0.1)$ for -2.3 < [Fe/H] < -1.5. We proceed to discuss the stellar content of VII Zw 403 using evolutionary tracks as well as a classification scheme based on optical and near-IR colors, and comment on the detection of asymptotic giant branch stars and the Blue Hertzprung Gap. We use M_H as an indicator of M_{bol} for red stars after evaluating BC_H at low metallicity.

We calculate the fractional contribution of individual stars from our color-magnitude diagram to the integrated light of VII Zw 403 and determine which red stellar population dominates the integrated colors. We find that young red supergiants, and young and intermediate-age asymptotic giants, together provide about 50% of the light in I, J and H bands, whereas the old red giant stars contribute less than 15%. Young, main-sequence stars and blue supergiants account for the remaining light and dominate in V. This explains the difficulties in discerning the nature of Blue Compact Dwarf galaxies when only integrated photometry is available.

Subject headings: Galaxies: compact — galaxies: starburst — galaxies: dwarf — galaxies: evolution — galaxies: individual (VII Zw 403 = UGC 6456) — galaxies: stellar content — stars: color-magnitude diagrams, infrared radiation — stars: evolution

1. Introduction

Blue Compact Dwarf galaxies (BCDs) are defined by their low luminosities ($M_B \ge -18$), blue spectra with narrow emission lines, small optical sizes, large H-I mass fractions (Thuan & Martin 1981), and low oxygen abundances in their ionized interstellar gas (e.g., Izotov & Thuan 1999). BCDs are known locally ($z \approx 0.02 - 0.03$), with a few as far as $z \approx 0.1$ (Thuan et al. 1994). They are among the most vigorously star-forming dwarfs in the nearby Universe.

The study of stellar populations in BCDs is interesting for several reasons. First, ever since their discovery, it has been an open question whether BCDs are "young" galaxies which are forming their dominant stellar population at the present epoch, or "old" galaxies which formed their first generation of stars earlier and are currently rejuventated by a starburst (Searle & Sargent 1972). What is the nature of the BCDs?

Second, dwarf galaxies are the most common kind of galaxy at the present epoch (e.g. Marzke & da Costa 1997), and they may have been even more numerous in the past (Ellis 1997). Guzmán et al. (1998) propose that the (type CNELG = Compact Narrow Emission Line Galaxy) faint blue galaxies at redshifts of $z \approx 0.5$ could be luminous BCDs that are experiencing a strong starburst. The ensuing supernova explosions are hypothesized to blow out the entire gas supply, resulting in a rapid fading through passive evolution (e.g., Dekel & Silk 1986, Babul & Ferguson 1996). However, HDF-N observations do not see the large numbers of faint red dwarf galaxy remnants predicted by this scenario (Ferguson & Babul 1998). What happened to the faint blue excess in the last few Gyr?

This paper addresses the star-formation history (SFH) of BCDs. The stellar content of BCDs provides a fossil record of their SFHs. However, most BCDs are at such large distances that only their most luminous stars can be resolved, even with the HST.

VII Zw 403 is a very nearby (4.5 Mpc) example of the BCD class. It is a key object to study with HST since it is close enough to be well resolved into individual stars (Schulte-Ladbeck et al. 1998, hereafter SCH98; Lynds et al. 1998). VII Zw 403 is a type "iE" BCD in the classification of Loose & Thuan (1986). This is by far the most common type of BCD, and is considered characteristic of the BCD phenomenon. The outer isophotes of iEs are elliptical, whereas the brightest star-forming regions are distributed somewhat irregularly in the vicinity of the center — although not at the exact center. This description is strikingly similar to that of early-type (dSph, dIrr/dSph) galaxies in the Local Group (see Mateo 1998). VII Zw 403 exhibits a smooth, elliptical background sheet (see the R-band image of Hopp & Schulte-Ladbeck 1995) with an integrated color consistent with an old and metal poor stellar population (Schulte-Ladbeck & Hopp 1998). The background sheet resolves in HST/WFPC2 images into individual red giant stars. The scale length derived from the resolved stars is about 50% larger than that of the large spheroidals of the Local Group. Schulte-Ladbeck et al. (1999, hereafter SHCG99) propose that VII Zw 403 posseses an old underlying stellar population. This supports earlier suggestions that all BCDs showing extended halos of red color might be old galaxies. It also strengthens the possible evolutionary link between BCDs and early-type dwarfs (e.g., Sung et al. 1998). VII Zw 403 has a present-day metallicity of about $Z_{\odot}/20$ (see SHGC99), a moderate star-forming rate of $0.013~{\rm M_{\odot}yr^{-1}}$ (Lynds et al. 1998), a large H-I mass of about $7{\rm x}10^7~{\rm M_{\odot}}$ (SHCG99), an extended H-I envelope (Thuan 1999, private communication), and a large outflow of hot gas detected in X-rays (Papaderos et al. 1994). Therefore, VII Zw 403 is clearly in the process of cycling gas in and out of the deepest part of its gravitational potential; this may regulate its star-formation rate and promote transitions in optical morphology between early and late type over Gyr time-scales.

VII Zw 403 has an H-I derived heliocentric velocity of -92 km/s (Tully et al. 1981). Tully et al. combined this with the fact that VII Zw 403 is somewhat resolved in their

ground-based images to associate it with the M81 group, at an assumed distance of 3.25 Mpc. When we applied the tip-of-the-red-giant-branch (TRGB) method to derive its distance from the I-band luminosity function of the halo stars, we found that VII Zw 403 is about 40% further away, at about 4.5 Mpc (SHCG99). A survey of several emission-line galaxy catalogs (e.g., Kunth & Sèvre 1986, Thuan & Martin 1991, Terlevich et al. 1991, Salzer et al. 1995, Pustil'nik et al. 1995, Popescu et al. 1996 and references therein) reveals additional BCDs with small positive recession velocities corresponding to the 5 to 10 Mpc distance range. We selected another four well studied BCD/dIrrs for NICMOS observation, and these will be discussed in future papers (Hopp et al. 2000).

Near-IR observations have already been used to investigate the nature of BCDs. Tully et al. (1981) observed VII Zw 403 in J and H in an aperture centered on the starburst, and attributed the near-IR flux to red supergiants. Thuan (1983, 1985) obtained integrated, near-IR photometry of a large sample of BCDs and argued that he had found an old population of K and M giants. Unfortunately, as Thuan (1983) recognized, it is difficult to discriminate between a population of young red supergiants and one of old red giants using only the total optical/infrared colors of a star-forming galaxy, because of the overlap in the effective temperature ranges of red supergiants and red giants. Campbell & Terlevich (1984) obtained photometric CO indices of BCDs and asserted that the population detected in the near-IR is primarily composed of supergiants from the current starburst. Subsequent near-IR imaging has been used to resolve the more centrally concentrated star-forming regions which are dominated by the younger supergiants, from the more extended background sheets, which are potentially dominated by older red giants (e.g., James 1994, Vanzi 1997, Davies et al. 1998). However, James (1994) found that intermediate-age, asymptotic giant branch (AGB) stars could be responsible for as much as 50% of the near-IR emission of some BCDs, further complicating the interpretation of near-IR data in terms of stellar populations. Whereas integrated colors and color profiles

of mixed-age stellar populations yield ambiguous results, it is in principle possible to distinguish among contributions from young red supergiants (RSGs), intermediate-age AGB stars, and stars on the first ascent red giant branch (RGB) with the help of color-magnitude diagrams (CMDs).

There is little work in the literature regarding resolved stellar populations of similar star-forming galaxies in the near-infrared. The local starburst cluster R 136 in the 30 Dor region of the LMC has been studied with adaptive optics in the near-IR, but there is no old population (Brandl et al. 1996). NIC2 results on R 136 (Walborn et al. 1999) focus on the young, and still embedded, massive stars. Adaptive optics, near-IR photometry has not yet been applied successfully to the study of stellar populations in the more distant star-forming galaxies of the Local Group (e.g., Bedding et al. 1997). The DeNIS survey which is currently in progress at ESO, is mapping the Magellanic Clouds (MC) simultaneously in I, J, and K_s , to limiting magnitudes of about 18, 16 and 14, respectively. DeNIS data clearly reach below the TRGB, as evidenced by preliminary color-luminosity diagrams and luminosity functions published by Cioni et al. (1999). In addition, the CMDs are well populated with blue stars, presumably the upper main sequence and blue supergiants. Recently, the post-starburst dIrr IC 10 and the dIrr IC 1613 were resolved in J and H with limiting magnitudes of J \approx 18 and H \approx 17.5 (Borissova et al. 1999). These data are considered deep enough to show the TRGB (m-M = 24.0 and 24.2, or distances of a few hundred Kpc, respectively). However, inspection of their luminosity functions shows the suspected TRGB occurs at the very limit of their data where incompleteness due to crowding is a severe problem. The dIrr galaxy NGC 3109, at a distance of m-M = 25.6 or 1.4 Mpc (Alonso et el. 1999), is located in the outer regions of the Local Group. Alonso et al. observed it in the near-IR to limiting magnitudes of about 20 and 19 in J and H. The RGB is below the detection limits in the near-IR.

There are no known BCDs in the Local Group. Much deeper limiting magnitudes and better spatial resolution are required if we wish to resolve the old stars in galaxies at distances of up to 10 Mpc (m-M = 30.0). In order to reach the TRGB in such BCDs, we can make use of recent improvements in near-IR imaging. The peak of the spectral energy distribution of RGB stars occurs in the near-IR. A K5 giant, for example, has colors of V-I = 2.1 (Johnson 1966) and V-H = 3.5 (Koornneef 1983), suggesting that a significant gain of near-IR over optical imaging is possible. Near-IR observations are therefore a promising route to mining the old stellar populations in BCDs at large distances. The NICMOS instrument aboard HST offered the opportunity to study stellar populations in the near-IR at high spatial resolution and deep limiting magnitudes. VII Zw 403, for which optical and near-IR single-star photometry is discussed in this paper, provides the "proof of concept." Hopp et al. (2000) give a preview of our intended applications to the additional four galaxies observed by us with HST/NICMOS.

Here we present near-IR images of VII Zw 403 obtained with HST's NIC2 camera. The galaxy is resolved into single stars in the near-IR, several magnitudes deeper than previously achieved for dIrrs from the ground, and sufficiently deep to yield useful measurements of stellar magnitudes and colors. We compare these measurements with WFPC2 observations of the same galaxy, to form an empirical characterization of the stellar content in the near-IR. We measure the TRGB in the HST equivalents of the J and H bands, and provide a calibration of the TRGB method. In future publications, we will apply these TRGB fiducials to NICMOS observations of other resolved BCD and dIrr galaxies for which there are no optical TRGB data. We compute the fractional light that different stellar types contribute to the integrated colors in optical and near-IR bands. Finally, we comment on the nature of BCDs.

2. Observations and reductions

The star-forming regions of VII Zw 403 are located near the center of an elliptical background-light distribution (Hopp & Schulte-Ladbeck 1995, Schulte-Ladbeck & Hopp 1998). In the HST/WFPC2 observations with which we compare our NICMOS photometry, the star-forming centers are situated in the PC chip. An image of this region was published as Plate 1 of SCH98. The three WF chips cover part of the elliptical background-light distribution of VII Zw 403, but, due to the geometry of the arrangement of the WF chips, not the entire galaxy. A record of the UV/optical imaging obtained with the WFPC2 on 1995 July 7 in F336W, F555W, F814W, and F656N filters, the equivalent of the U, V, I and H α passbands, was given in SCH98. Errors and completeness fractions for stellar photometry in the continuum bands, and comments on the transformation into the Johnson-Cousins system can be found in SHCG99.

2.1. NICMOS imaging

NICMOS observations of VII Zw 403 were obtained on 1998 July 23 as part of GO program 7859. Information about the observations can be gleaned directly from the STScI WWW pages linked to this program ID.

The NICMOS instrument houses three cameras, the NIC1, NIC2 and NIC3, in a linear arrangement. Data for VII Zw 403 were obtained with all three cameras operating simultaneously, to mitigate some of the detector problems which became known during the phase-II stage of the proposal. However, although all three detectors were collecting photons, not all three yield data which are useful for this study. The NIC3 cannot be brought into focus simultaneously with NIC1 and NIC2, and even NIC1 and NIC2 are not completely confocal. We conducted the observations at the compromise focus position

between NIC1 and NIC2. We performed all of our imaging observations in the F110W and F160W filters, the rough equivalents of the J and H bands. Although our primary goal was to obtain deep imaging with both high resolution and large area coverage of regions located in "Baade's red sheet ²", our observing strategy was designed to optimize the scientific return and minimize the risk of using a new instrument with somewhat uncertain performance. We therefore chose to locate the NIC2 chip, which has a larger area and higher sensitivity at lower resolution than the NIC1 chip, within the central starburst region of the galaxy rather than in the elliptical background sheet. In order not to constrain the schedulability of the observations limited by the lifetime of the NICMOS cryogen, we also decided not to request a specific orientation of the observations, and so the NIC1 chip was positioned within the outskirts of the background sheet of VII Zw 403 at that spacecraft roll which happened to occur on the observing date. The geometry of the NICMOS observations relative to the WFPC2 observations can be gleaned by comparing Figure 1 to Plate 1 of SCH98. For reference, the NIC2 camera has a field of view of 19.2"x19.2" and a pixel scale of 0.075". Thus the area of the NIC2 is only about 30% of the area of the PC.

The observations were split into several exposures and read out in MULTIACCUM mode. The parameters were chosen to address several issues which are laid out in the NICMOS documentation (detector read-out noise, saturation of bright sources, amplifier glow), and to optimally fill the total time available per HST orbit. From one exposure to the next, the NICMOS camera was dithered in the X direction. This procedure allowed for a better sampling of the PSF, better flux measurements, and the removal of cosmic rays and background in the processing of the data.

²The term "Baade's red sheet" has its roots in Baade's foundation of the stellar population concept, i.e., the definition of Population I and II. An interesting historical perspective on his ideas was given by Sandage (1986).

Due to its sensitivity and very small field of view, the NIC1 camera produced images which contain very few point sources. We will not discuss the NIC1 data in this paper. The NIC3 images exhibit several bright stars, but the stellar images are out of focus. Therefore, we will not discuss the NIC3 data in this paper either.

In the F110W filter, we gathered a total of six individual exposures, three having integration times of 1023.95 sec each, and three of 767.96 sec. Severe cosmic-ray persistence in the images (see below) convinced us not to include one of the short exposures in the final dataset. The total integration time for the F110W image is therefore 4607.77 sec. In the F160W filter, we took a total of five exposures, each with an integration time of 767.96 sec. Again, one of the datasets was so badly affected by cosmic-ray persistence that we chose not to add it into the final image. The integration time of the F160W filter image used here is therefore 3071.84 sec.

The NIC2 observations were reduced with the latest reference files available in the calnical pipeline, and the individual observations were combined into a mosaic with the calnicb pipeline. However, this reduction was not satisfactory. The data showed surprisingly few point sources compared to the WFPC2 images. They displayed a high and spatially non-uniform background. Aperture photometry immediately indicated that the anticipated limiting magnitudes were not achieved. In fact, initially the DAOPHOT (Stetson, Davis & Crabtree 1990) software did not recognize many of the point sources visible by eye.

The observations of VII Zw 403 are severly affected by what are known as the "pedestal" and the "cosmic-ray persistence" problems. Both of these problems result in the addition of spatially non-uniform, high backgrounds to the data, preventing the detection of faint stellar IR point sources in our images.

We are very grateful that Dr. M. Dickinson allowed us to use his personal software to remove to a large extent the effect of the pedestal-induced background in our data. To accomplish removal of the pedestal, the raw data were first run through the calnica pipeline without applying a flat-field correction. We then used MD's software to interactively fit a pedestal-free sky level to the background in the four quadrants of the NIC2 detector. The data were re-processed through calnica with the flat-field flag on. The individual exposures so reduced exhibited a much smoother and a lower background than the raw data.

In order to avoid the cosmic-ray persistence, we had requested that our data be obtained well away from the South Atlantic Anomaly; however, this was not possible due to the pressure on NICMOS time and the ensuing scheduling difficulties during its short lifetime. Because all of the exposures are affected by this problem at some level, the final data do not reach as deeply as they would otherwise.

We proceeded to combine the reduced data with calnicb. However, careful inspection of the mosaiced images revealed that the PSF of the point-sources varied noticably across the images. Since DAOPHOT photometry is sensitive to the shape of the PSF, we needed to minimize these PSF variations. To do this, we combined our distortion-corrected exposures using a drizzling routine, instead of using the calnicb pipeline, (which, at time of our data reduction, did not take into account geometric distortion.) The drizzling process required a careful manual masking of detector blemishes before the image combination.

The resulting images in F110W and F160W have a more uniform and lower background, and a more uniform and rounder PSF, than the data reduced by the pipeline. Owing to the dithering procedure, areas at the edges of the images in X direction have a lower signal-to-noise, which we trimmed off.

2.2. Single-star photometry on NICMOS images

The NIC2 single-star photometry is the result of an iterative process. After the images were reduced as described above, we fitted a PSF to about one hundred fairly isolated sources in each image and carried out photometry. We set the zeropoint using the most recent photometric keywords available for the F110W and the F160W filters used with NIC2. We examined about a dozen sources in each image to calculate the aperture correction that we applied to the DAOPHOT PSF photometry. The CMD in F110W, F160W reached deeply enough to reveal the TRGB. However, the photometric errors for the faint sources were large.

Therefore, we once again examined the background. The background was still non-uniform due to imperfect pedestal correction, the remaining cosmic-ray persistence, and bound-free and free-free emission from ionized gas in the H-II regions. Smaller photometric errors for the faint sources were obtained when the background was smoothed with a 23x23 pixel median filter after all the identified point sources were removed from the data. Photometry on this background yielded smaller photometric errors for the stars that were previously identified by DAOPHOT, and as a consequence, a tighter distribution of the stars on the CMD. While an even more extended sea of very faint sources was visible on the images by eye before the background smoothing was applied, the high photometric errors on the sources that were identified with DAOPHOT convinced us that photometry of these potentially real, faint red giants was not feasible. The images which had the smoothed background subtracted off are shown in Figure 1.

When we overlayed the sources identified by DAOPHOT on the images, we noticed that the extended PSF, especially in the F160W filter, yielded multiple identifications of very bright sources. Possibly as a result of the pedestal removal and the drizzling, the first diffraction ring was of a non-uniform brightness, and DAOPHOT identified parts of the

ring as 3-4 additional point sources. These sources were usually several magnitudes below the main peak and had a high error. However, more severly, we noticed that in several cases the main core of the PSF of the brightest stars was identified with two PSFs of equal brightness. After much experimentation with the PSF and other clipping parameters within DAOPHOT, we found that the best results were achieved when the images were smoothed with a 3x3 pixel filter. In this way the sizes of the cores of the PSFs were degraded slightly to a FWHM of 2.9 pixels (0.22") in F110W and 3.6 pixels (0.27") in F160W, but the brightness distribution in the diffraction features was more uniform. An illustration is provided in Fig. 2. We reapplied DAOPHOT and the bright stars were found as single sources, while the sources erroneously identified as faint stars within the PSFs of the bright stars vanished. With this procedure we measured 2134 individual sources with residual errors smaller than 0.55 mag in F110W, and 1500 sources in F160W. In constructing the CMD we required spatial coincidence of the sources to within 3 pixels; 998 such sources were found.

Finally, we re-investigated the photometry of the stars used for the photometric calibration and the aperture correction. By measuring these stars in a series of ever larger circular apertures, we found that the PSF had not been encompassed sufficiently by the 0.5" aperture. We calculated an aperture correction to the 0.5" aperture (for which the photometric conversion is given by the NICMOS photometric calibration) and re-applied the appropriate corrections to the data sets.

In Fig. 3, we display the internal errors of the photometry. The errors for F110W exceed 0.1 mag for a magnitude of 23.7; for F160W they reach 0.1 mag at a magnitude of 22.5. We performed completeness tests using the same procedure described in SHCG99. In Fig. 4, we summarize the results. The data are nearly complete (>95% of test stars recovered) for magnitudes <23; completeness drops to 50% at 25.4 in F110W and 24.1 in

F160W.

3. Results and Discussion

The WFPC2 CMD in V and I contains 5459 sources, and is displayed as Fig. 5. Throughout most of this section, the $[(V-I)_o, M_{Io}]$ CMD serves as a guide to interpreting the NICMOS results. Main-sequence (MS), blue supergiant (BSG), blue-loop (BL), RSG, AGB and RGB stars are all represented. This CMD is extensively discussed in SCH98, Lynds et al. (1998) and SHCG99; we have good knowledge of the location of various stellar phases on this diagram.

Figure 5 shows the evolutionary tracks with Z=0.0004; Z=0.004 ($Z_{\odot}/50$ and $Z_{\odot}/5$, respectively) from the Padova library (Fagotto et al. 1994). These have been transformed into the observational (HST) plane by using bolometric corrections and color tables (Origlia & Leitherer 2000) produced by folding the HST filter/system response with model atmospheres from Bessell, Castelli & Plez (1998) with [M/H] = -1.5; [M/H] = -0.5. These transformation tables adopt $M_{V,\odot} = 4.83$ (e.g. $M_{bol,\odot} = 4.75$, $BC_{V,\odot} = -0.08$) and colors equal to zero for the model atmosphere representing α Lyrae. The F555W and F814W magnitudes of these two grids were transformed to Johnson-Cousins V and I magnitudes in the ground system using Table 10 of Holtzman et al. (1995), so that the tracks are on the same photometric system as the VII Zw 403 observations.

In Fig. 5, we overlay a few tracks of either metallicity onto the observations. The tracks nicely illustrate the well-known age-metallicity degeneracy of the RGB in broad-band colors, i.e., the tip of the first-ascent red giant branch of the Z=0.0004, 1 M_{\odot} model which has an age of about 7 Gyr virtually coincides with that of the Z=0.004, 4 M_{\odot} model which has an age of about 160 Myr, in the [(V-I)_o, M_{Io}] plane. Thus, additional arguments based

on the positional dependence of the RGB were employed in SHCG99 to suggest the presence of an old and metal-poor stellar population.

A CMD of the near-IR photometry is displayed as Figure 6, in terms of instrumental magnitudes in the Vega system. A transformation of the F110W and F160W photometry into J and H is attempted below. Since additional systematic errors are added in the process, we first discuss the F110W and F160W photometry. The foreground extinction towards VII Zw 403 (E(B-V) = 0.025) is negligible at the central wavelengths of the near-IR filters (computed using Cardelli, Clayton & Mathis 1989). Because VII Zw 403 is situated at high Galactic latitude, and the NIC2 camera has a very small size, the contribution to the CMDs by Galactic foreground stars is also negligible.

The NIC2 images were situated well within the PC images of VII Zw 403. We cross-identified sources found in both cameras by transforming the NIC2 coordinates into the WFPC2 system. We then merged our photometry lists, and investigated the distribution of stars on a variety of color-color diamgrams and CMDs. There are 549 sources found in V, I, J, and H.

3.1. Two-color diagrams and internal extinction

We examined two-color diagrams (TCDs) for all combinations of the data sets (Figure 7). The TCDs show two clumps of stars corresponding to the blue and red plumes of the CMDs (see below), with only a few sources located outside of this main distribution of stars. The reddening vectors are approximately parallel to the distribution of stars even using our seemingly advantageous long color baseline of V-F110W vs. V-F160W. This can also be seen in Koornneef (1983), Fig. 1, for ground-based V, J, H data. We do not discuss TCDs involving the U band here, due to the paucity of sources found in U and the near-IR

bands.

We investigated the reason for observing a few sources off the main clumps of stars in the TCDs, and found that the deviant data points can all be explained by large photometric errors (> 0.1 mag) in one of three filters. We thus attribute the sources which are offset from the main distribution to measurement error and not to internal reddening. This result of undetectable internal reddening in VII Zw 403 is consistent with the seemingly unreddened location of the blue plume in the $[(V-I)_o, M_{Io}]$ CMD, centered on 0 mag, and with the fact that few stars change position from the red to the blue side when we plot CMDs with a larger color baseline (see below).

Furthermore, Lynds et al. (1998) derived E(B-V) = 0.04–0.08 for the internal extinction of stellar associations in VII Zw 403. This corresponds to $A_V = 0.12$ –0.25, and, using the Galactic extinction law of Cardelli, Clayton & Mathis (1989), translates into $A_J = 0.03$ –0.07 and $A_H = 0.02$ –0.05. As expected, the extinction in the near-IR is very small.

3.2. Luminosity functions in the near-IR and the TRGB method for deriving distances

Briefly, the TRGB method (Lee et al. 1993) makes use of the relative insensitivity to metallicty of M_{bol} of the tip of the first-ascent red giant branch, as well as the insignificance of line-blanketing for the I magnitude of metal-poor red giants, and the availability of well-calibrated bolometric corrections to the I band based on the V-I color of the RGB. However, similar calibrations for the F110W or F160W filters do not exist. Furthermore, as illustrated in Fig. 8, while the absolute I magnitude at the TRGB is constant below an [Fe/H] of about -0.7, those in J and H display a metallicity dependence. In this section, we discuss an empirical near-IR TRGB calibration based on the VII Zw 403 data, which is

therefore valid for the VII Zw 403 metallicity. In the following sections, we will investigate the dependence of the near-IR TRGB on metallicity both empirically and using models.

In SHCG99, we derived the distance modulus of VII Zw 403 to be $(m-M)_o=28.23$ from the V-I color of the RGB for the halo population combined with the location of the TRGB in the I-band. This immediately allows us to place an absolute magnitude scale on the near-IR CMDs of VII Zw 403, to identify the TRGB here, and to interpret the stellar content of the near-IR CMDs. The RGB is clearly distinguishable in the near-IR CMDs, as expected, as a densely populated region at red colors and faint magnitudes, the red tangle.

Comparing Fig. 5 with Fig. 6 we notice that, while showing great morphological similarity, the near-IR CMDs do not exhibit the pronounced red tail of AGB stars seen in the optical CMD. In the near-IR CMDs, the red plume continues into the red tangle as a strikingly linear feature with colors 0.75 < (F110W-F160W) < 1.5. The RSG, AGB and RGB stars are not well-separated in color, as we further illustrate below. However, tracing along the red plume it is also evident that a vast increase in the star counts occurs at faint magnitudes, and a TRGB can be distinguished from these data.

Luminosity functions in F110W and F160W were derived by counting stars in 0.1 mag bins in the color interval 0.75<(F110W-F160W)<1.5. As Fig. 9 shows, the luminosity functions display a sharp rise of the star counts towards fainter magnitudes. We identify this rise with the TRGB. We emphasize that the TRGB occurs at apparent magnitudes in F110W and F160W where the completeness of our data is still very high (above 90%). Using the above distance modulus, we find the TRGB is located at

$$M_{F110W,TRGB} = -4.28 \pm 0.10 \pm 0.18$$
 and $M_{F160W,TRGB} = -5.43 \pm 0.10 \pm 0.18$,

where errors were computed from a combination of the random and systematic errors as

discussed in SCH98.

The near-IR TRGB values are presumably valid at the metallicity of the halo population of VII Zw 403, namely at $\langle [\text{Fe/H}] \rangle = -1.92 \pm 0.04$ ($\text{Z}_{\odot}/83$). We compare the empirical values with the 15 Gyr TRGB in our low-metallicity grid (evolution at [Fe/H]=-1.7, atmospheres at [Fe/H]=-1.5, see above) and find that the models yield $M_{F110W,TRGB} \simeq -4.6$ and $M_{F160W,TRGB} \simeq -5.6$, in good agreement with the data.

These results provide one "calibration" for the TRGB in the near-IR, and could in principle be applied to other galaxies with old and similarly metal-poor giant branches. We now discuss the accuracy of the method by comparing our CMD in J and H to those of globular clusters (GCs).

3.3. Transformation to J and H

The STScI NICMOS team supplies on their home page data for five standard stars (release Nov. 25, 1998), including magnitudes in HST filters and standard ground-based filters. This small sample consists of a white dwarf, a G star, and three red stars of increasingly redder color. The total color range of the stars is $-0.04 \le \text{J-H} \le +2.08$ and the total magnitude range is $7.3 \le \text{H} \le 12.7$. The ground-based data of the NICMOS standard stars are mostly unpublished (private communication from the NICMOS IDT to the STScI NICMOS team). At least one red star comes from the list of Elias et al. (1982; CIT system of JHK magnitudes). The STScI NICMOS team mentions discrepancies of the order of 0.1 mag between the ground-based data in their Table and those of Persson et al. (1998, LCO system; see this paper and references therein for a comparison of the various ground-based systems). A complete transformation into a ground system is not yet available.

We used the data of the NICMOS team to establish transformation equations from the F110W, F160W magnitudes and color to the ground-based system, applying a simple linear least-squares fit to the data:

$$J-H = (0.035 \pm 0.14) + (0.758 \pm 0.061) * (F110W - F160W)$$

 $H = (-0.001 \pm 0.06) + F160W - (0.091 \pm 0.027) * (F110W - F160W)$

The errors give the quality of the fit but of course do not take into account any of the systematics (such as the offset mentioned above, or the limited sampling of color range by the few standards). It is therefore difficult to estimate the uncertainties introduced by applying these transformations. We have to assume that the accuracy is no better than 0.1 mag, and probably worse.

In Fig. 10, we display the CMDs of VII Zw 403 in J and H. Overlayed are the tracks for the same stellar masses and metallicites as we used in Fig. 5. The tracks were transformed to the ground-system using the above equations. There is no major qualitative change in these CMDs as compared to those in the instrumental system (cf., Fig. 6). Quantitatively, the main effect is a shift of the red plume towards the blue plume. An advantage of transforming the data into the JHK system is that our CMDs and luminosity functions can be more readily compared with the few available ground-based data of similar galaxies in the near-IR (see Alonso et al. 1999, Borissova et al. 1999, Cioni et al. 1999). The transformation also enables a comparison of our data with ground-based photometry of GCs in the Milky Way and the LMC. We can also give the J, H magnitudes of the TRGB of VII Zw 403 (see Table 1).

In making comparisons of near-IR data sets, additional offsets may be encountered because the various ground-based observations were obtained in different realisations of the JHK filter system. For a careful comparison, we need to transform all of the data into the same system. Persson et al. (1998) extend the bright near-IR standard star measurements of Elias et al. (1982) to fainter magnitudes. They discuss how the LCO system compares to others (UKIRT, see Casali & Hawarden, 1992; CTI, see Elias et al., 1982, AAO, see Bessel & Brett, 1988) and find rather good agreement between the UKIRT, CTI, and LCO systems in H and K. The J band is less straightforward. For instance, Elias et al. (1983) derive transformation formulae between the AAO system and their CTI system. Again, H and K show good agreement and the two systems can be treated as identical systems for our purposes. However, a significant transformation coefficient (about 0.8 mag) has to be taken into account for J. This may be due to the large contribution of atmospheric features in this band. In our discussion below, we shall therefore focus our comparisons on the H-band results, where the three systems discussed above can be assumed to be identical within the accuracy of our transformation to the ground system.

3.4. TRGB H magnitudes in GCs and stellar models

If we wish to use the VII Zw 403-derived calibration as a distance indicator for other galaxies, we have to investigate the sensitivity to metallicity of the TRGB luminosity in the near-IR. To study this limitation of our estimator, we followed two approaches, using both stellar evolution models and GC data for guidance.

First, we read off the magnitudes from the Padova isochrones (Bertelli et al. 1994, see also Fagotto et al. 1994) for 15 Gyr old stars for the largest available metallicity range. These data are shown in Fig. 8. Bertelli et al. provide their isochrones in the Johnson-Cousins system in the optical and in the near-IR passbands defined by Bessel & Brett (1988, AAO system).

The I-band shows the well-known quasi-constant absolute magnitude level for

metallicities, [Fe/H], below -0.7. According to the models, the absolute J-band magnitudes are brighter than the I ones (an advantage) but also vary strongly, displaying a rapid monotonic increase with [Fe/H] (a disadvantage). The H-band magnitudes offer the advantage of being about 2 mag brighter, on average, than M_I . Unfortunately, the models indicate a complex dependence between [Fe/H] and the TRGB in H. M_H exhibits a plateau at about -6, in the range -0.4>[Fe/H]>-1.3. Fig. 8 thus suggests that an H-band TRGB might be useful at slightly higher metallicities than that for which the I-Band TRGB is applicable. However, towards the very low metallicities of interest for us, M_H suddenly changes by about 0.4 mag. Furthermore, the theoretical isochrones barely approach the metallicity regime of our dwarf galaxy data. VII Zw 403 in particular lies below the lowest metallicity point covered by published models (see Fig. 11). (We add that we also investigated the TRGB magnitudes in our two grids, which use the Bessell, Castelli & Plez (1998) atmospheres rather than pure Kuruzc atmospheres adopted in the Padova grids, and that they agree to within 0.05 mag).

Second, we compiled JHK data of GCs in the Milky Way and the LMC from the literature. These data cover a large metallicity range. We used the observed CMDs to read off the magnitudes at the TRGB; together with the GC distances, this yields another indication of the dependence of the absolute TRGB magnitudes on metallicity. The major difficulty of this approach is that frequently, the empirical RGBs of GCs are not sufficiently populated near the tip to provide a reliable tip magnitude. Other sources of error include uncertainties in the GC distances and metallicities.

Kuchinski et al. (1995, a, b) observed several GCs of the Milky Way belonging to the so-called disk system. These have [Fe/H] metallicities between -1 and 0. The authors also discuss older data for 47 Tuc and M 71. From these published CMDs, we read off the K magnitudes of the TRGBs, and their H-K colors, to derive H-TRGB magnitudes. We

adopted the distance moduli and extinction corrections as presented by Kuchinski et al. to derive absolute H-TRGB values for these nine clusters. Kuchinski et al. use the Elias et al. (1982) standards for the CTI system. As they are interested in disk clusters, extinction is a severe problem for some of the data sets, especially for M 71 and Ter 2. The Kuchinski et al. cluster data have only a small overlap in [Fe/H] with the dwarf galaxies we are interested in. But, they serve as a comparison with the models at high metallicity.

Ferraro et al. (1995) presented ground-based JHK photometry of stars in 12 GCs of the LMC. The data are in the CTI system of Elias et al. (1982). Unfortunately, the sampling at the TRGB is so poor in most of these clusters, that a secure determination of the TRGB magnitude in either of the near-IR colors is not possible. Furthermore, only some of the GCs observed by Ferraro et al. have published [Fe/H] values, and these have rather large uncertainties. We finally used only four of their GCs (see Fig. 11). The LMC clusters also have abundances which are higher than the range of interest for us, but, together with the Kuchinski et al. results, they allow an independent check of the results derived from the isochrones. There is a rather large dispersion in the observed data for these GCs (all with [Fe/H]≥-1), but they do cluster about the TRGBs of the isochrones, which is somewhat reassuring.

Recently, Davidge & Courteau (1999) observed four metal-poor Galactic halo GCs in the near-IR. They used the standard stars of Casali & Hawarden (1992) and supplied values of the TRGB in J, H, and K. The brighter parts of the RGBs are rather well sampled. The [Fe/H] values of these four clusters range from -2.3 to -1.5. These are in the range of interest for studies of metal-poor, old stellar populations in galaxies. Most importantly, they bracket the abundance of VII Zw 403 ([Fe/H] = -1.92). The two more metal-rich GCs of their sample overlap with the isochrone result, and there is good agreement between the models and the data. These four GCs indicate only a weak dependence of $M_{H,TRGB}$ on

[Fe/H] for small values of [Fe/H]. We use the four metal-poor GCs of Davidge & Courteau, the model TRGB value for 15 Gyr and Z=0.0004, and our data point for VII Zw 403, to derive $M_{H,TRGB}$. As can be seen from Fig. 11, a good approximation is

$$\langle M_{H,TRGB} \rangle = -5.5(\pm 0.1)$$

for -2.3 $\langle [Fe/H] \langle -1.5.$

We propose that this value may be used to derive the distances to dwarf galaxies containing metal-poor stellar populations, with sufficient accuracy to be useful for stellar-population studies.

We found disturbing the "downward" trend of $M_{H,TRGB}$ for low [Fe/H] suggested by the Padova isochrones, as compared with the "flattening" of $M_{H,TRGB}$ in the range from -2.3<[Fe/H]<-1.5 indicated by the observations. We therefore secured a stellar evolutionary grid at [Fe/H] = -2.3 from the Frascati group (Cassisi, private communication). The 14 Gyr isochrone of their stellar-evolution code yields $M_{H,TRGB} \approx$ -5.6 at [Fe/H] = -2.3. This provides a consistency check of our empirical result. We do not show this additional point in Fig. 8 and 11 since it is based on a different stellar evolutionary code as the one to which we compare our data throughout the remainder of the paper.

The TRGB is the preferred distance indicator when no observations of Cepheids are available, because its physics is well understood, and because when well calibrated (such as in the I band), it achieves a similar accuracy (Madore & Freedman 1998.) The large number of stars populating the near-IR CMDs of star-forming dwarf galaxies near the TRGB (cf. also, Hopp et al. 2000) indicates that the TRGB method does not suffer from the statistical uncertainty which is sometimes encountered when investigating GC ridgelines in the near-IR. Therefore, the transformation and calibration uncertainties are the dominant sources of error in using the near-IR TRGB as a distance indicator for these galaxies. This method is

superior to other distance indicators for galaxies in the 5-10 Mpc range; however, care must be taken not to mis-identify the tip-of-the-AGB (TAGB) with the TRGB. The method of the three brightest RSGs, on the other hand, is always severely affected by small-number statistics (Schulte-Ladbeck & Hopp 1998, Greggio 1986).

3.5. M_H as a measure of M_{bol} for red stars

Bessell & Wood (1984) investigated bolometric corrections for late-type stars. From observations of individual red giants and supergiants in the MWG, LMC, and SMC, they find $BC_H = 2.6(\pm 0.2)$. In other words, the empirical value for BC_H is derived to be independent of color or spectral type, and metallicity. In Figure 12, we show this empirical relation between M_H and M_{bol} as a straight line. An inspection of Fig. 5 in Bessell & Wood (1984) suggests the possibility that the lowest-metallicity data (those for the SMC stars) might be slightly below their recommended value, at a BC_H that is closer to 2.4, respectively.

To see how the recommendation of a constant BC_H by Bessell & Wood compares to theoretical expectations, we overlay in Figure 12 the locations of the TRGBs and TAGBs from the Padova isochrone library. Their near-IR photometry is in the same system as the data of Bessell & Wood. We again used the 15 Gyr isochrones over the range of available metallicities, and the values of M_H and M_{bol} associated with these red giant models. These points lie near the empirical calibration, but are clearly offset toward lower M_H for a given M_{bol} . The lowest metallicity point in the stellar-evolutionary models (Z=0.0004) corresponds to a BC_H of 2.1. In order to make a comparison at high luminosities, we use the theoretical luminosities at the tip of the AGB. We show the TAGB points for solar metallicity and one fifth of solar, and for ages from 150 Myr to 15 Gyr. As illustrated in Fig. 12, while the stellar models with solar metallicity follow well enough the empirical

relation, the lower-metallicity models are offset to a smaller M_H for a given M_{bol} .

The constancy of BC_H in Bessell & Wood is somewhat surprising, since observed giants will be located along the giant branches, and not just at the tips. In order to better understand how BC_H varies along the giant branches, we have investigated in detail our transformed tracks. It turns out that in the models, BC_H increases along the tracks and that it depends on the stellar mass (i.e. age of the population). These variations are particularly pronounced for the Z=0.004 grid, with BC_H at the tips ranging between 2.3 and 2.6, and between similar limits for the 0.9 M_{\odot} model in the brightest 1.5 mag of its RGB evolution. The situation improves slightly for the Z=0.0004 grid, where BC_H ranges between just 2.0 and 2.2 at the various tips, and within approximately the same limits for the 0.8 M_{\odot} model in the brightest 1.5 mag of its RGB evolution. A constant BC_H is not justified from the models, and the interpretation of transformations from the observational to the theoretical plane will require simulations, since there may be multiple choices for the theoretical parameters of any individual star given its observed color and magnitude.

In summary, for the low metallicities which occur in our objects, a smaller BC_H than that suggested by the data of Bessell & Wood appears to be more appropriate. While BC_H clearly varies strongly with stellar mass, at Z=0.0004 the TRGBs for models of a wide range of stellar masses can be approximated by a constant. We hence employ the following relation to characterize the dependence of M_H on M_{bol}

$$< M_{bol} > = M_H + 2.1(\pm 0.1)$$

for Z =0.0004

We use this relation to derive the bolometric luminosity function of the red stars in VII Zw 403 (Fig. 13.). This bolometric luminosity function is valid for the stars at the TRGB (in terms of metallicity, color or temperature, BC_H), but is only a rough

approximation (plus minus several thenths of a mag) for other stars. We caution that using a constant BC_H does introduce uncertainties in going from the observed to the theoretical plane, and that the interpretation of luminosity functions or HR diagrams (cf. also Alonso et al. 1999, Borissova et al. 1999) requires simulations.

The TRGB in Fig. 13 is measured to occur at a bolometric luminosity of -3.4(± 0.1). This agrees very well with the theoretically expected M_{bol} from Fig. 8. Our result also compares very well with preliminary results from the DeNIS project by Cioni et al. (1999), who find $M_{bol,TRGB}$ to be -3.4 for the LMC and -3.6 for the SMC. These data were transformed to M_{bol} using different relations as H is not one of the survey bands. The agreement is thus all the more encouraging.

We detect a large number of stars below the TRGB. Above the TRGB, the stellar numbers are small and thus highly affected by statistical errors. The bulk of stars which we observe in the luminosity range -3.4 > M_{bol} > -6.5 is compatible with these stars being largely AGB stars in VII Zw 403 (cf. also, Fig. 15). The data are consistent with the most luminous AGB stars being only a few hundred Myr of age, while the least luminous, oldest ones have ages of several Gyr. The four most luminous red supergiants span the luminosity range from approximately -6.5 > M_{bol} > -8.5. We note that the cool part of the Humphreys-Davidson limit, the upper luminosity boundary of RSGs, is thought to occur at M_{bol} of -9.5 (Humphreys & Davidson 1994). The uncertainties in the transformation from the observed to the theoretical plane prevent us from stating how close our most luminous, near-IR detected objects are to this boundary. A comparison of Fig. 14 with Fig. 5 reveals that, while we are missing some of the bright supergiants in the near-IR as compared to the optical, we do see the most luminous object, at M_I of about -9, so we are sampling the entire upper luminosity range. The reason why we miss in the near-IR a few of the brightest supergiants, is due to the fact that the area of the NIC2 chip covers less than a

third of the star-forming centers, while the PC chip encompasses these regions very well.

The total absolute blue magnitude of VII Zw 403 is small, about -14 (see Schulte-Ladbeck & Hopp 1998). At these small galaxy luminosities, fluctuations in the numbers of the most luminous and hence most massive stars are expected (Greggio 1986). Statistical effects have been known to be important in the UV and optical, and continue to be important for the interpretation of near-IR luminosity functions and CMDs. We discourage the use of the brightest RSGs as a distance indicator. Similarly, the comparative studies of the RSG populations of galaxies are severely affected by small-number statistics (cf. the stellar frequencies for $M_{bol} < -7$ in Fig. 17 of Massey 1998).

3.6. Decoding the near-IR CMDs

In Fig. 14, we color-code the main areas of the CMDs using terminology that an observer would employ to classify stars according to the different morphological features seen on the CMD. The classification is based on the $[(V-I)_o, M_{Io}]$ CMD of Fig. 5. The stars marked in blue are mainly MS and BSG stars; stellar evolutionary tracks tell us BL stars occur here as well. The stars indicated in magenta are considered to be RSG; the tracks suggest there may be BL stars at the faint end. More importantly, the tracks indicate bright AGB stars populate this part of the red plume as well, and we cannot easily differentiate them from RSGs. We are able to clearly distinguish AGB stars when they form the red tail; these stars are marked in black. Finally, we colored all of the data points which occur below the TRGB in red, suggesting that mainly RGB stars are found here. However, stellar evolution tracks indicate we must be aware of BL and faint AGB stars in this part of the CMD as well. With this broad classification of stars, we now compare the morphology of the optical—near-IR CMDs.

In Fig. 14, we use the stellar classification to investigate the stellar content of the $[(J-H)_o, J_o]$ and $[(J-H)_o, H_o]$ CMDs. This elucidates a problem which we alluded to earlier, namely that even those AGB stars which populate the redward-extended tail of optical CMDs overlap with the RSGs in near-IR CMDs. As we stated before, the colors of RSG, AGB and RGB stars are quite degenerate with respect to $(J-H)_o$ color, or temperature. Folded with the color errors that arise from the measurements, only luminosity can help us distinguish between RSG and bright AGB stars on the one hand, and RGB (plus faint AGB stars) on the other hand. At the top of the red plume, we can distinguish the most luminous RSGs from the bright AGBs based on luminosity (AGB stars are not expected at an M_{bol} of -8, cf. Fig. 12). We notice from Fig. 14 some mingling of faint stars between blue and red colors. This is most pronounced for stars below the TRGB. Above the TRGB. only a few stars are seriously "misplaced" based on optical color in the near-IR CMDs. We also note that our placement of the TRGB derived from the luminosity functions in F110W and F160W is consistent with our stellar classification scheme. In other words, no stars classed RGB stars based on the $[(V-I)_o, M_{Io}]$ migrated above the TRGB limit in the near-IR CMDs, while just a few stars classed RSG or AGB stars wander below the TRGB. Hence, there is an overall good agreement between the TRGB magnitudes based on stellar classification and the luminosity functions.

We may ask what kind of stars are we missing in the optical CMDs which are present in near-IR CMDs. Comparing Fig. 14 with Fig. 10, some differences for faint stars are apparent, in the sense that some faint stars of extreme color in Fig. 10 do not appear in Fig. 14. This is not unexpected as objects that are extremely red may have been missed in the optical, and objects that are extremely blue may be blends or spurious detections in the near-IR. There is very good agreement for the brightest, and hence most luminous objects – it appears that none of the brightest supergiants seen in J and H were not seen in V and I as well, giving some confidence that we have a complete sample of the brightest

supergiants that were encompassed by the NIC2 chip's area in the near-IR. The only potentially significant difference then between Fig. 10 and 14 occurs in the color range $(J-H)_o > 1.1$. Five stars are found here with very red colors, and with brightnesses above the TRGB. They have small measurement errors and must be considered to be real. In this parameter space, we thus picked up additional objects in the near-IR photometry. It is possible, judging from their colors, that these objects are Miras or Carbon stars.

In Fig. 15, we show a CMD that uses the I and H bands. It may be compared with Fig. 5 which employs the I and V bands. Fig. 15 illustrates that our expectations for observing in the near-IR were realized: the H-band allowed for an over 1 mag gain in stellar brightnesses for the red stars. The tracks cross the data in slightly different places on the $[(V-I)_o, M_{Io}]$ and the $[(I-H)_o, M_{Ho}]$ planes, with offsets of a few tenths of a mag. These discrepancies are not too surprising considering the uncertainties in the transformations from the space to the ground systems on the one hand, and the difficulties of model atmospheres to reproduce empirical color-temperature relations on the other hand. They suggest that the state-of-the-art for comparing empirical and synthetic CMDs is to reproduce the gross features of the stellar distibutions including the absolute magnitude of the TRGB quite well, whereas other quantitative results such as e.g., metallicities from the location of the RGB, or detailed SFHs, should be considered somewhat more uncertain.

3.7. Long color-baseline CMDs

We now present and interpret CMDs with long color baselines. Fig. 16 shows the CMDs of I_o or M_{Io} versus $(V-I)_o$, $(V-J)_o$, and $(V-H)_o$. The same color scheme as that used for Fig. 14 is employed; however, notice the change in color scale. These CMDs in principle offer advantages for separating out different stellar phases from one another. In practice, since the photometric errors vary from band to band and depend on the colors of

the objects, the potential of these CMDs to distinguish different stellar phases is not fully realized.

An impressive feature of the CMDs of Fig. 16 is the increasingly larger spread of the data in color. For instance, the data points in the $(J-H)_o$ CMD of Fig. 10 subtend only about 1.5 mag, those in the $(V-I)_o$ CMD already cover 4.5 mag. In $(V-J)_o$ this baseline has grown to about 6.5 mag, and in $(V-H)_o$, the data are distributed over a range of almost 8 mag.

As we study CMDs with increasing color baseline, the color errors at the faint end of the stellar distributions become very large. Therefore, for the faint magnitudes, we observe some mingling of stars across the CMDs. We do not consider this to be a real effect. Only one bright star migrates from the red plume of the $(V-I)_o$ CMD into the blue plume of the $(V-H)_o$ CMD. This could potentially be a heavily reddened blue object, or else a blend of unresolved objects weighted very differently in different colors.

The red plume of the $(V-I)_o$ CMD was considered to be composed of RSGs plus AGBs mainly in a narrow region where it appears to form a linear sequence from low to high luminosity. Stars offset to red colors from this band were classed AGBs only. Comparing the three CMDs with each other, we see that we judged quite well from the $(V-I)_o$ CMD the location of the AGB. Two luminous objects considered RSGs based on the $(V-I)_o$ CMD might also be classed AGB stars based on the $(V-H)_o$ CMD. At least half a dozen or so of the faint red stars near the dividing line between the RSG, AGB, and RGB stars in the $(V-I)_o$ CMD could be additional AGB stars based on the $(V-H)_o$ CMD. In Fig. 14, two BSGs wandered from the blue plume into the red plume of the CMDs, demonstrating further difficulties to disentangle the nature of red stars in this luminosity range based on CMDs.

A feature of the four brightest RSGs detected in all four bands is that they appear to

develop a progressively larger redward color offsets in the $(V-J)_o$ and $(V-H)_o$ CMDs from the linear band that was used to class them as RSGs on the $(V-I)_o$ CMD. Since these are bright objects with small measurement errors, we assume that this effect is real. We do not expect to see AGB stars at such high luminosities, and so must assume that these colors are intrinsic to the most luminous RSGs sampled by the NIC2 frame.

A significant spreading out of colors occurs for the bluest stars and stars between the MS and the RSG plume/red tangle; presumably high- and intermediate-mass stars on blue loops. This is in part due to high measurement errors for blue objects in the near-IR bands. The effect of differential reddening could play a role in this re-distribution of sources, but we cannot constrain it on the basis of our data.

3.8. Comments on the Blue Hertzsprung Gap and the blue-to-red supergiant ratio at low metallicity

An interesting feature of the optical/near-IR CMDs of Figs. 14-16 is the appearance of a gap in the distribution of stars along the blue plume. We first noticed this in the optical, PC data centered on the star-forming regions of VII Zw 403 (SCH98). We interpret this gap as the Blue Hertzsprung Gap (BHG) which is predicted by stellar-evolution theory, to occur between the distribution of massive stars at the red edge of the MS (core-H burning) and the blue edge of the BL phase (core-He burning).

Simulations of the VII Zw 403 CMD with the code of Greggio et al. (1998), which use the low-metallicity grid also employed in this paper, were presented in SHCG99. The synthetic CMDs shown as Fig. 6 in SHCG99 display the predicted BHG for young ages of the stellar population. In comparing Fig. 6 of SHCG99 with the CMDs presented in this paper, it appears that the BHG occurs at a lower luminosity in the models than that feature

which we identify with the BHG in the data. This difference can readily be explained recalling that the simulations were carried out for stellar evolution at Z=0.0004 ($Z_{\odot}/50$). The extent of the BLs in stellar evolution models is very sensitive to metallicity. In Fig. 15, we connect with a straight line the locations of the blue edges of the blue loops for the 20 and the 9 M_{\odot} tracks in the Z=0.0004 and the Z=0.004 ($Z_{\odot}/5$) grids. These nicely bracket the location of the observed BHG. The appearance of the BHG between the tracks of these two grids is consistent with the metallicity of the ionized gas of VII Zw 403, which suggests the present generation of stars has metallicities closer to $Z_{\odot}/20$. In future simulations, we will incorporate into the code the Z=0.001 metallicity grid, as well as all the bands now available from observations.

The BHG is seen very well in the CMD of the nearby Local Group dIrr Sextans A (Dohm-Palmer et al. 1998 and references therein), for which the WFPC2 photometric errors are even smaller in the $[(V-I)_o, M_{Io}]$ CMD than those for the more distant VII Zw 403. The oxygen abundances for Sextans A ($\log (O/H) = -4.48$, Skillman 1989) and VII Zw 403 $(\log (O/H) = -4.42(0.06), Martin 1997, and -4.31(0.01), Izotov, Thuan & Lipovetsky 1997)$ are quite similar, around $Z_{\odot}/20$. A gap in the distribution of stars was not seen in the H-R diagram of the slightly metal-poor $(Z_{\odot}/3)$ LMC by Fitzpatrick & Garmany (1990). Since it was predicted by stellar-evolution theory, its absence in these data gave rise to the problem of the missing BHG (e.g. the reviews of Maeder & Conti 1994 and Chiosi 1998). Theoretical work has therefore been aimed at filling in the "missing" BHG with stars, for instance by developing and incorporating into the theory of stellar evolution new prescriptions for internal mixing and/or mass loss in massive stars (Salasnich, Bressan, & Chiosi 1999). We note that the BHG is now also being discovered in CMDs of the LMC (Zaritsky 1999, private communication) which are being assembled as part of the digital Magellanic Could Photometric Survey (Zaritsky, Harris & Thompson 1997). These data will give insight into why the BHG was not observed by Fitzpatrick & Garmany (1990); first suspicions include

the smaller sample size and the spatial distribution of stars across the LMC.

The fact that the BHG has now been seen in the CMDs of several metal-poor galaxies indicates that more observational work on the HR diagrams of metal-poor star-forming galaxies is needed, and that such CMDs may provide important guidance for stellar-evolution theory. They suggest that additional mixing and mass-loss may not be needed to the extent currently anticipated by theorists.

A related issue is the blue-to-red supergiant ratio in galaxies. Recent reviews/papers on this open problem of massive-star evolution are those of Langer & Maeder (1995) and Deng, Bressan & Chiosi (1996). In brief, the B/R supergiant ratio as a function of Z has not yet been predicted consistently by stellar-evolution models. However, the data being used to address this problem largely date back quite some time now, to the excellent series of papers by Humphreys et al. on the supergiant stellar content of Local Group galaxies (e.g., Humphreys & McElroy 1984). Our data allow us to contribute a new measurement at low-metallicity, but only in a limited way; again, small-number statistics rules. Since the largest problems for predicting the B/R ratios generally occur at low metallicities, the limited insight gained here may nevertheless be useful.

Owing to the visibility of the BHG on the CMDs, we are quite well able to separate the core-H burning MS from the core-He burning BSG stars. Counting stars in the various CMDs shown in this paper yields a number of about 20±3 BSGs, with an RMS error of 4. We anticipate that the largest systematic error arises from preferrentially missing BSGs due to crowding in the star-forming centers; this would have the effect of increasing the B/R ratio. Assessing the number of (core-He burning) RSGs turns out to be more difficult. This is owing to the already much deliberated fact that it is difficult to discern massive RSGs from intermediate-mass, AGB stars. This is true for our photometry as well as for the other existing data sets which attempt to address the B/R ratio (Brunish, Gallagher &

Truran 1986). Based on their high luminosity we can clearly identify 4 stars with RSGs. In this case, assuming the counts are dominated by the RMS errors in the stellar numbers, the B/R ratio for VII Zw 403 is 5 ± 4 . This ratio is consistent with the SMC ($Z_{\odot}/10$) numbers (cf. Langer & Maeder 1995). If additional stars in the red plume of VII Zw 403 are true red supergiants in the evolutionary sense, then the ratio goes down. This demonstrates the large effects that statistical and systematic errors have in affecting empirical assessments of the B/R supergiant ratio.

3.9. From CMDs to integrated photometry — implications for detecting old stellar populations

In this section, we perform an exercise aimed at clarifying the interpretation of integrated photometry of BCDs. For this purpose, consider the NIC2 chip to be a single aperture photometer of about 19" x 19" centered on the active star-formation regions of the BCD. As discussed in the previous section, HST single-star photometry and stellar-evolution tracks allow us to distinguish broadly the main different stellar phases on the CMDs of VII Zw 403. We add the light of stars in different phases to investigate their contributions to the total light in the V_o , I_o , I_o , and I_o bands. In other words, we perform population synthesis based on single-star colors and luminosities.

The results of the summation are shown in Table 2. We divide the stars into three categories: stars in the blue plume (MS, BSG and BL stars), red stars above the TRGB (RSG and bright AGB stars), and red stars below the TRGB (RGB stars, some faint AGB stars, and possibly some BL stars). Among the stars below the TRGB, the dominant population is considered to be RGB stars. However, depending on the age and early SFH of this BCD (which we cannot completely determine from the morphology of the red tangle alone) there may also be faint AGB stars. Because we are positioned on the star-forming

centers, some faint BL stars might contribute here; for the less massive stars, the blue and red portions of their evolution are not as widely separated on our diagrams as those for the more massive stars.

Looking at Table 2, one simple result is clear: A few luminous stars outshine even a large number of faint stars. The light in an aperture centered on the star-forming regions is dominated in the I_o , J_o , and H_o bands by RSG and luminous AGB stars. These obviously outshine the older RGB stars. The MS, BSG and BL stars belonging to the young and blue population are also significantly brighter in all three near-IR bands than the old stellar population. The sea of red giants so well resolved with HST contributes less than 15% to the integrated light in any of these filters.

Notice also that three quarters of the light in V_o comes from the young, blue stars, and less than 10% from the evolved stars, reinforcing the results of Schmidt, Alloin & Bica (1995) that even a small mass fraction of young stars superimposed on the background sheet of a dwarf Elliptical (dE) or dSph galaxy will completely outshine and render undetectable the underlying old population in optical passbands.

Our results have implications for the integrated photometry of BCDs in general. The actively star-forming regions of BCDs are the visually brightest regions. Aperture photometry, including that in the near-IR (e.g. Tully et al. 1981, Thuan 1983, 1985), was traditionally carried out with photometric apertures centered on these bright H-II regions. The apertures used were usually about 10" in size, thus encompassing mainly the star-forming centers. As our exercise suggests, such observations are dominated by the young (less than about 50 Myr old) red supergiants from the most recent star formation activity and by luminous AGB stars with ages less than a few Gyr. We concur with James (1994), that luminous AGB stars must be considered an important component of BCDs, contributing around half of the light in the star-forming region, and reflecting star-forming

activity in the last few Gyr.

It is therefore not possible to conclude, from integrated photometry centered on the starburst alone, whether an underlying, old (>10 Gyr) stellar population is present. Since even the near-IR bands predominantly measure the light from the younger stars, forming colors such as V-J or V-H which involve long baselines does not help to break this ambiguity.

In Schulte-Ladbeck et al. (2000), we address the possibility to use spectrophotometric indices based on long-slit spectra that exclude the star-forming regions (see Hopp, Schulte-Ladbeck & Crone 1998) in order to age-date the background sheets of BCDs. This method has its roots in the work on spectrophotometric dating of Elliptical galaxies (e.g. Worthey 1994); and while it suffers from its own ambiguities, it may represent an important alternative to single-star photometry for dating distant BCDs in the future.

The morphological properties of VII Zw 403 are representative of the vast majority of BCDs. We have previously demonstrated (SHCG99) the presence of a "core-halo" morphology for the resolved stars in this galaxy. Young stars are exclusively found in the core near the center of the extended light-distribution of the halo (approximately in the inner 40"). At large radii (out to 100" or about 4 disk scale lenghts), this young population is absent, but we find some AGB stars and a very strong red tangle dominated by RGB stars. As discussed in Schulte-Ladbeck & Hopp (1998), stellar population synthesis of integrated colors in the outer halos of BCDs (using color gradients derived from multi-filter surface photometry) suggest that even here, a mixed-age population (resulting from a complex SFH) is consistent with the data. In the case of VII Zw 403 where we know from single-star photometry that bright RSGs are absent in the halo, we have interpreted the halo color profile as evidence for the presence of an underlying population which is at least a few Gyr old (and possibly truly ancient, > 10 Gyr old). It is likely that the halos of other iE BCDs are similarly composed of old and/or intermediate-age stars.

One of the most interesting implications of our results here; however, is that those BCDs which do *not* exhibit an outer halo, do not necessarily lack old stars. It is entirely possible that their star forming regions are scattered through an older populations, totally obscuring it.

4. Summary and Conclusions

The quality of the NICMOS photometry in terms of crowding and limiting magnitudes represents an improvement by several apparent magnitudes over exisiting ground-based near-IR data of similar galaxies. In terms of absolute magnitudes, comparable data are only available for the MCs. The results of our single star photometry demonstrate that all of the important stellar phases of composite stellar populations can be traced on near-IR CMDs. The optical/near-IR CMDs of VII Zw 403 show the "missing" Blue Hertzsprung Gap and a blue-to-red supergiant ratio of about 5, providing new input for stellar-evolution models at low metallicity.

Several steps could be undertaken to improve our analysis: 1) Modeling of stellar atmospheres and stellar evolution at the low metallicities appropriate for the earliest stellar populations in dwarf galaxies, 2) Additional modeling and observations of the AGB stellar phase, to better understand the effects of AGB ages and metallicities, 3) Near-IR observations providing a uniform set of cluster CMDs in a well-established JHK system, for comparison of such simple stellar populations with stellar theory and galaxy observations.

Our data reach the RGB of VII Zw 403 to completeness levels that allow a secure measurement of the J, H magnitudes at the tip. We compare our results to that of clusters, DeNIS data of the MCs, and the Padova tracks of stellar evolution, and give a conversion from apparent to absolute TRGB magnitude. Providing a TRGB fiducial in the near-IR has

advantages for estimating the distances to more distant galaxies. As red giants are observed near the peak of their energy distributions, the near-IR TRGB method can potentially reach to further distances than the optical TRGB method. It may also prove useful for highly reddened galaxies.

The bolometric luminosity function of the red stars shows that for any stellar component other than the red giants, the RMS error in the star counts is large, even in the near-IR. Statistical fluctuations in stellar numbers in low-luminosity galaxies are well known to become large for massive stars. We caution against using the method of the brightest red supergiants as a distance indicator even in the near-IR.

Summing up the light of the resolved stars in different evolutionary phases, we illustrate that published integrated photometry of BCDs, in both the optical and the near-IR, is dominated by the light from luminous, young red supergiants from the current starburst (the last 50 Myr or so) and luminous young and intermediate-age AGB stars. Attempts to distinguish an old stellar component using near-IR colors are bound to fail because of the color degeneracy among RSG, AGB, and RGB stars. Even a large number of red giants is undetectable underneath just a few luminous RSG and/or AGB stars. This shows why contradicting conclusions have been reached in the literature regarding the oldest stellar components of BCDs.

The purpose of our study is to use SFHs to answer very general questions about the nature of BCDs: Are they "young" galaxies? Are they related to the faint blue excess? We note that AGB stars are clearly identified in the resolved stellar content, and also contribute significantly to the integrated near-IR light of VII Zw 403. The presence of an intermediate-age stellar population suggests that star formation was active in this galaxy at times which correspond to reshifts of a few tenths. VII Zw 403 is clearly not a young galaxy. We argue that the AGB stars may provide a further link between the type iE BCDs

and the faint-blue galaxy population. The trick will be to determine whether or not this component of AGB stars can correctly account for the right amount of star formation at the right time, to identify iE galaxies as the (non-merged) remnants of the (CNELG) faint blue excess.

In conclusion, we present the first exploration of the near-IR CMD of a BCD galaxy, to deep enough limiting magnitudes to detect the evolved descendents of low-mass stars. Together with recent results regarding the structural parameters of BCDs (e.g. Sung et al. 1998), our data provide further support of the idea that type iE BCDs possess dynamically relaxed, old stellar populations. The nature of the iE BCDs is inferred to be one of flashing dEs/dSphs. An interrelated evolution between BCDs and dEs/dSphs galaxy types (via gas cycling through starbursts) could potentially account for precursors as well as remnants of the faint blue galaxies.

We acknowledge financial support through archival HST research grants to RSL (AR-06404.01-95A, AR-08012.01-96A) and guest observer HST grants to RSL and MMC (GO-7859.01-96A). This project benefitted from the hospitality of the Universitätssternwarte München, where RSL found a stimulating environment during her sabbatical leave from the University of Pittsburgh. We are grateful to Dr. M. Dickinson for sharing his time and software to help us remove the pedestal in the NICMOS data. We also thank D. Gilmore for excellent support during our visit to STScI. We further thank Dr. L. Origila for sharing her HST magnitudes of the Bessell, Castelli & Plez (1998) stellar atmospheres with us prior to publication. UH acknowledges financial support from SFB375.

REFERENCES

Alonso, M.V., Minniti, D., Zijlstra, A.A., Tolstoy, E. 1999, A&A, 346, 33

Allen, D.A., Cragg, T.A. 1983, MNRAS, 203, 777

Babul, A., Ferguson, H.C. 1996, ApJ, 458, 100

Bedding, T.R., Minniti, D., Courbin, F., Sams, B. 1997, ApJ, 495, L13

Bertelli, G., Bressan, A., Chiosi, C., Fagotto, F., Nasi, F. 1994 A&AS, 106, 275

Bessell, M.S., Brett, J.M., 1988 PASP, 100, 1134

Bessell, M.S., Castelli, F., Plez, B. 1998, A&A, 333, 231

Bessell, M.S., Wood, P.R., Brett, J.M., Scholz, M. 1991, A&AS, 89 335

Bessell, M.S., Wood, P.R. 1984, PASP, 96, 247

Borissova, J., Georgiev, L., Rosado, M., Kurtev, R., Bullejos, A., Valdez-Guiterrez, M. 1999, A&A preprint (astro-ph/9903019)

Brandl, B., Sams, B.J., Bertoldi, F., Eckart, A., Genzel, R., Drapatz, S., Hofmann, R., Loewe, M., Quirrenbach, A. 1996, ApJ, 466, 254

Brunish, W.M., Gallagher, J.S., Truran, J.W. 1986, AJ, 91, 598

Campbell, A.W., Terlevich, R. 1984, MNRAS, 211, 15

Cardelli, J.A., Clayton, G.C., Mathis, J.S. 1989, ApJ, 345, 245

Casali, M., Hawarden, T. 1992, JCMT-UKIRT Newsl., No. 4, 33

Chiosi, C. 1998, in "Stellar Astrophysics for the Local Group", eds. A. Aparicio, A. Herrero, and F. Sánchez (Cambridge University Press), p. 1

Cioni, M.R., Habing, H.J., Loup, C., Groenewegen, M.A.T., Epchtein, N., and the DeNIS Consortium 1999, in IAU Symp. 192, "The Stellar Content of Local Group Galaxies", eds. P. Whitelock, R. Cannon, (PASP: IAU) p. 65 Davies, R.I., Sugai, H., Ward, M.J. 1998, MNRAS, 295, 43

Davidge, T. J., Courteau, S. 1999, AJ, 117, 1297

Deng, L., Bressan, A., Chiosi, C. 1996, A&A, 313, 159

Dohm-Palmer, R.C., Skillman, E.d., Saha, A., Tolstoy, E., Mateo, M., Gallagher, J., Hoessel, J., Chiosi, C., Dufour, R.J. 1998, AJ, 115, 152

Dekel, A., Silk, J. 1986, ApJ, 303, 39

Ellis, R.S. 1997, ARA&A, 35, 389

Elias, J.H., Frogel, J.A., Matthews, K., Neugebauer, G. 1982, AJ, 87, 1029

Elias, J. H., Frogel, J. A., Hyland, A. R., Jones, T. J. 1983, AJ, 88, 1027

Fagotto, F., Bressan, A., Bertelli, G., Chiosi, C. 1994, A&AS, 104, 365

Ferguson, H.C., Babul, A. 1998, MNRAS, 296, 585

Ferraro, F.R., Fusi Pecci, F., Testa, V., Greggio, L., Corsi, C.E., Buonanno, R., Terndrup, D.M., Zinnecker, H. 1995, MNRAS 272, 391

Fitzpatrick, E.L., Garmany, C.D. 1990, ApJ, 363, 119

Greggio, L. 1986, A&A, 160, 111

Greggio, L., Tosi, M., Clampin, M., De Marchi, G., Leitherer, C., Nota, A., Sirianni, M. 1998, ApJ, 504, 725

Guzmán, R., Jangren, A., Koo, D.S., Bershady, M.A., Simard, L. 1998, ApJL, 495, 13

Holtzman, J.A., Burrows, C.J., Casertano, S., Hester, J.J., Trauger, J.T., Watson, A.M., Worthey, G. 1995, PASP, 107, 1065

Hopp, U., Schulte-Ladbeck, R.E. 1995, A&AS, 111, 527

Hopp, U., Schulte-Ladbeck, R.E., Crone, M.M. 1998, in Bonn/Bochum-Graduiertenkolleg Workshop, ed. T. Richtler & J.M. Braun (Shaker Verlag), 161 Hopp, U., Schulte-Ladbeck, R.E., Greggio, L., Crone, M.M. 2000, Proc. STIS Workshop on "Spectrophotometric Dating of Stars and Galaxies", eds. I. Hubeny, S. Heap, and R. Cornett (PASP), in press

Humphreys, R.M., Davidson, K. 1994, PASP, 106, 1025

Humphreys, R.M., McElroy, D.B. 1984, ApJ, 284, 565

Izotov, Y.I., Thuan, T.X., 1999, ApJ, 511, 639

Izotov, Y.I., Thuan, T.X., Lipovetsky, V. 1997, ApJS, 108, 1

James, P.A. 1994, MNRAS, 269, 176

Johnson, H.L. 1966, ARA&A, 4, 193

Koornneef, J. 1983, A&A, 128, 84

Kuchinski L.E., Frogel, J.A., Terndrup, D.M., Persson, S. E. 1995, AJ, 109, 1131

Kuchinski, L.E., Frogel, J.A. 1995, AJ, 110, 2844

Kunth, D., Martin, J.M., Maurogordato, S., Vigroux, L. 1986, in "Star-Forming Dwarf Galaxies and Related Objects", eds. D. Kunth, T.X. Thuan, and J. Tran Than Van (Gif-sur-Yvette: Éditions Frontières), 89

Kunth, D., Sèvre, F., 1986, in "Star-Forming Dwarf Galaxies and Related Objects", eds. D.
Kunth, T.X. Thuan, and J. Tran Than Van (Gif-sur-Yvette: Éditions Frontières),
331

Langer, N., Maeder, A. 1995, A&A, 295, 685

Lee, M.G., Freedman, W.L., Madore, B.F., 1993 ApJ, 417, 553

Loose, H.H., Thuan, T.X. 1986, in "Star-Forming Dwarf Galaxies and Related Objects", eds. D. Kunth, T.X. Thuan, and J. Tran Than Van (Gif-sur-Yvette: Éditions Frontières), 73

Lynds, R., Tolstoy, E., O'Neil Jr., E.J., Hunter, D.A. 1998, AJ, 116, 146

Maeder, A., Conti, P.S. 1994, ARA&A 32, 227

Martin, C. 1997, ApJ, 491, 561

Marzke, R.O., Da Costa, L.N. 1997, AJ, 113, 185

Massey, P. 1998, ApJ, 501, 153

Mateo, M. 1998, ARA&A, 36, 435

Origlia, L., Leitherer, C. 2000, AJ, submitted

Papaderos, P., Fricke, K.J., Thuan, T.X., Loose, H.-H. 1994, A&A, 291, L13

Persson, S. E., Murphy, D.C., Krzeminski, W., Roth, M., Rieke, M.J. 1998, AJ, 116, 2475

Popescu, C.C., Hopp, U., Hagen, H.J., Elsässer, H. 1996, A&AS, 116, 43

Pustil'nik, S., U., Gryumov, A.V., Lipovetsky, V.A., Thuan, T.X., Guseva, N. 1995, ApJ, 443, 499

Salasnich, B., Alessandro, B., Chiosi, C. 1999, A&A, 342, 131

Salzer, J.J., Moody, W.J., Rosenberg, J.L., Gregory, S.A., Newberry, M.V. 1995, AJ, 109, 2376

Sandage, A. 1986, ARA&A, 24, 421

Schmidt, A. A., Alloin, D., Bica, E. 1995, MNRAS, 273, 945

Schulte-Ladbeck, R.E., Crone, M.M., Hopp, U. 1998, ApJ, 493, L23 (SCH98)

Schulte-Ladbeck, R.E., Hopp, U. 1998, AJ, 116, 2886

Schulte-Ladbeck, R.E., Hopp, U., Crone, M.M., Greggio, L. 1999, ApJ, in press (SHCG99)

Schulte-Ladbeck, R.E., Hopp, U., Crone, M.M., Greggio, L. 2000, in "Spectrophotometric Dating of Stars and Galaxies", ed. I. Hubeny, S. Heap & R. Cornett (PASP), in press

Searle, L., Sargent, W.L.W. 1972, ApJ, 173, 25

Skillman, E.D. 1989, ApJ, 347, 883

Stetson, P.B., Davis, L.E., Crabtree, D.B. 1990, in "CCDs in Astronomy", ed. G.H. Jacoby (PASP), 289

Sung, E.-C., Han, C., Ryden, B.S., Chun, M.-S., Kim, H.-I. 1998, ApJ, 499, 140

Terlevich, R., Melnick, J., Masegosa, J., Moles, M., Copetti, M.V.F. 1991, A&AS, 91, 285

Thuan, T.X. 1983, ApJ, 268, 667

Thuan, T.X. 1985, ApJ, 299, 881

Thuan, T.X., Izotov, Y.I., Lipovetsky, V., Pustilnik, S.A. 1994, in ESO/OHP Workshop on "Dwarf Galaxies", eds. G. Meylan & P. Prugniel (Garching: ESO), 421

Thuan, T.X., Martin, G.E. 1981, ApJ, 247, 823

Tully, R.B., Boesgaard, A.M., Dyck, H.M., Schempp, W.N. 1981, ApJ, 246, 38

Vanzi, L. 1997, PASP, 109, 1069

Walborn, N., Barbá, R.H., Brandner, W., Rubio, M., Grebel, E., Probst, R.G. 1999, AJ, 117, 225

Worthey, G. 1994, ApJS, 95, 107

This manuscript was prepared with the AAS IATEX macros v4.0.

Figure Captions

Fig. 1.— The NIC2 images after pedestal removal and re-calibration are displayed on the left, with F110W on top and F160W at the bottom. The horseshoe-shaped H-II region and the highly inclined background spiral help to identify the area covered by the NIC2 images w.r.t. the WFPC2 images, cf., Plate 1 of SCH98 for our color image of the UV/optical PC data. The images on the right illustrate the appearance of the images after background-smoothing was applied; a smooth background is essential for DAOPHOT single-star photometry.

Fig. 2.— Zooming in on the images in the F110W (top) and F160W (bottom) filters. On the left, the original PSF of the images is retained, on the right, the images on which we did the photometry, with PSF smoothing applied.

Fig. 3.— The photometric errors computed by DAOPHOT.

Fig. 4.— The fraction of test stars recovered on the NIC2 chip.

Fig. 5.— Color-magnitude diagram of the WFPC2 observations in V and I, corrected for foreground extinction. Overplotted are selected Padova tracks for a metallicity of Z=0.0004 and Z=0.004. The salient morphological features of this CMD are the blue plume, which contains MS, BSG, and BL stars, and the red plume, which at high luminosities, is comprised of RSG and AGB stars, and at low luminosities, becomes the well populated red tangle which contains RGB, low-luminosity BL, and low-luminosity AGB stars. The extended red tail is comprised only of AGB stars.

Fig. 6.— Color-magnitude diagrams of near-IR magnitudes in the Vega system. All stars found in F110W and F160W (998) are plotted. The near-IR CMDs exhibit a blue plume, as well as a red plume with a densely populated red tangle at low luminosities. An extended red tail is not seen.

Fig. 7.— Two-color diagrams for various combinations of optical and near-IR photometry. The points shown have photometric (1 σ) errors smaller than 0.15 mag.

Fig. 8.— The absolute magnitudes at the TRGB were read off from the 15 Gyr isochrones of the Bertelli et al. (1994) stellar models for metallicities of (from left to right), Z=0.0004, 0.001, 0.004, 0.008, 0.02, 0.05. The color-coding from top to bottom gives the tips in H (black), J (red), I (magenta), and bolometric (blue) magnitudes.

Fig. 9.— The luminosity functions in F110W (top) and F160W (bottom) for stars with 0.75<(F110W-F160W)<1.5. The location of the TRGB is marked.

Fig. 10.— Color-magnitude diagrams of near-IR magnitudes using the transformations described in the text. The bottom panel has overplotted the same tracks as those used in Fig. 5.

Fig. 11.— The absolute magnitude at the TRGB derived for VII Zw 403 (in red) is compared with those of stellar models (in green) and of globular clusters (in black). The open circles are clusters from Ferraro et al., no error bars are indicated owing to the difficulty of reading off the TRGB. The filled circles above [Fe/H] of -1 are from Kulchinski et al.; here, it was possible to estimate an error bar. The error bars reflect how well the RGB is populated near the tip, and how well, as a consequence, we felt that we could determine the location of the TRGB from these data. The points at low metallicities are the cluster data of Davidge & Courteau; we adopted their errors.

Fig. 12.— The relationship between M_H and M_{bol} for red stars. The straight lines come from Bessel & Wood (1984) and represents their fit to data and associated error bars of observations of a variety of red giants and supergiants in the Galaxy and the MCs. In green, we display the TRGBs of the Bertelli et al. (1994) 15 Gry isochrones for the full range of metallicities. The lowest metallicity point is the one with the smallest M_H ; and it suggest a

bolometric correction of 2.1. To extend the luminosity range, we also read off the tips of the AGBs on model isochrones. We did this for isochrones of two different metallicities, solar and one fifths of solar, and for ages ranging from about 150 Myr to 15 Gyr. An extensive discussion of the bolometric corrections derived from individual stellar models of different masses is provided in the text.

Fig. 13.— The absolute, bolometric luminosity function, as derived from the H-band luminosity function and using a constant to transform from M_H to M_{bol} (see the text). Notice that the use of a constant bolometric correction introduces substantial (of order of several tenths of a mag) uncertainties. A unique mapping of observational data onto the theoretical plane may not be possible, and solutions need to be investigated with simulations. The feature that can be interpreted fairly securely is the TRGB at $M_{bol} = -3.4$, as we set up our transformation to be appropriate for these stars.

Fig. 14.— Application of the stellar classification scheme based on the optical CMD to the near-IR CMDs. We use color-coding to illustrate the location of specific stellar-evolutionary phases. The color-coding is discussed in the text, and the labels given in the top CMD reflect what we judged to be the main stellar contributor to each morphological feature based on this CMD. The location of the TRGB is marked by a dashed green line. Only stars detected in four colors are shown. Although we observe a limited number of stars to cross the TRGB line in luminosity, in general, there is good agreement between the TRGB location as derived based on the luminosity functions and the location of the TRGB as indicated by our stellar classification scheme. We can also see that the RSG and AGB stars overlap closely in color and to a large degree, in luminosity as well, on near-IR CMDs.

Fig. 15.— Color-magnitude diagram of near-IR colors with the same tracks as those used in Fig. 5 overplotted. An absolute-magnitude scale in terms of M_H is provided as well. Comparing this CMD with that of Fig. 5 illustrates how well our expectations were realized

– we gained a little over 1 mag by observing the red stars in near-IR. We marked by thick bars the connecting points of the blue edges of the BL phases for the 20 (left) and the 9 (right) M_{\odot} stellar models in the two metallicity grids. They bracket the gap in the blue plume also seen in Figs. 13 and 15. This gap is interpreted to be the "missing" Blue Hertzsprung Gap.

Fig. 16.— Color-magnitude diagrams of stars found in all four bands. The I magnitude provided the original TRGB distance scale and the TRGB shown by the dashed green line is on the original absolute magnitude scale. The progressively longer color baselines illustrate how different stellar phases can in principle be well separated using near-IR colors, even for early-type stars. In practice, the errors for stars of different color vary sufficiently across the three CMDs to counteract some of these advantages in the present data set.

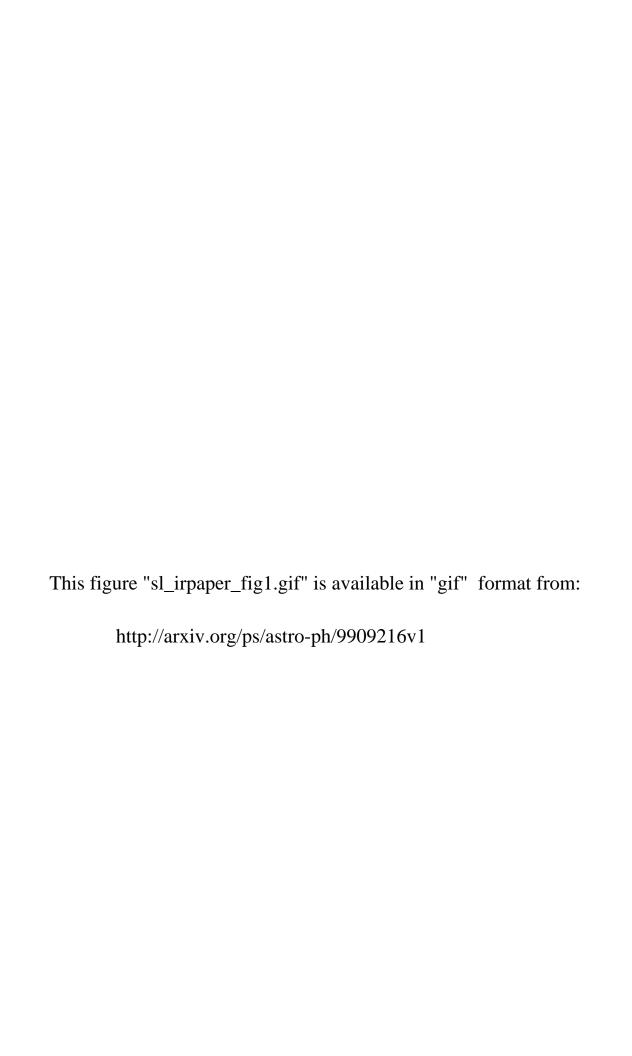


Table 1. THE TIP OF THE RED GIANT BRANCH IN THE NEAR-IR

(calibrated for the VII Zw 403 RGB at $<\![\mathrm{Fe/H}]\!>=-1.92)$

| Band | m_{TRGB} | ${\rm M}_{TRGB}^{-1}$ |
|-------------------------------|---------------------|---------------------------|
| I_0 | 24.25 ± 0.05^2 | $-3.98 \pm 0.09 \pm 0.18$ |
| $\mathrm{F}110\mathrm{W}_0$ | 23.95 ± 0.05^2 | $-4.28 \pm 0.10 \pm 0.18$ |
| $\mathrm{F}160\mathrm{W}_{0}$ | 22.80 ± 0.05^2 | $-5.43 \pm 0.10 \pm 0.18$ |
| J_0 | 23.60 ± 0.11^3 | $-4.63 \pm 0.15 \pm 0.23$ |
| H_{0} | 22.69 ± 0.11^3 | $-5.54 \pm 0.15 \pm 0.23$ |

 $^{^{1}\}mathrm{The}\ total\ random\ and\ systematic\ errors\ follow\ SCH98\ for\ I_{0},$ this paper for the near-IR colors.

 $^{^{2}\,\}mathrm{The}$ errors quoted are the read-off errors at the tip.

 $^{^3}$ The error quoted includes the minimum error of the space-to-ground transformation.

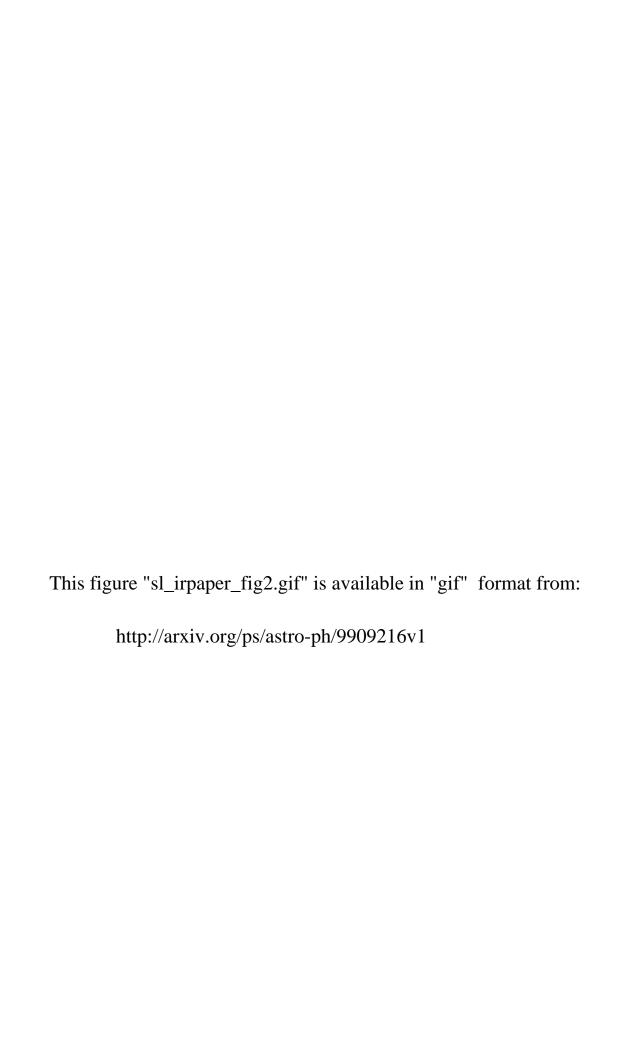


Table 2. INTEGRATED PHOTOMETRY OF THE NIC2 CHIP CMD in an \approx 19" x 19" aperture on the central starburst

| Stellar component | V-light (%) | I-light (%) | J-light (%) | H-light (%) |
|---|-------------|-------------|-------------|-------------|
| Blue plume (MS, BSG & BL stars) | 74 | 46 | 32 | 21 |
| Red plume above TRGB (RSG & bright AGB stars) | 18 | 42 | 55 | 63 |
| Red tangle (RGB & faint AGB stars) | 7 | 12 | 13 | 15 |

